Dielectric relaxation of water inside a single-walled carbon nanotube

Yuan Lin,[1,*] Junichiro Shiomi,[2,†] Shigeo Maruyama,[2] and Gustav Amberg[3]
[1]*Department of Process Technology, SINTEF Materials and Chemistry, Alfred Getz vei 2, Trondheim 7034, Norway*
[2]*Department of Mechanical Engineering, The University of Tokyo, 7-3-1 Hongo, Bunkyo-ku, Tokyo 113-8656, Japan*
[3]*Department of Mechanics, Linné FLOW Center, Royal Institute of Technology, Osquars Backe 18, Stockholm 100 44, Sweden*
(Received 27 February 2009; published 22 July 2009)

We report a molecular dynamics study of anisotropic dynamics and dielectric properties of water confined inside a single-walled carbon nanotube (SWNT) at room temperature. The model includes dynamics of an SWNT described by a realistic potential function. A comparison with simulations assuming a rigid nanotube demonstrates that the popular assumption severely overestimates the dielectric constant for small diameter SWNTs. Simulations of water inside flexible SWNTs with various diameters reveal strong directional dependence of the dynamic and dielectric properties due to the confinement effect. The obtained dielectric permittivity spectra (DPS) identify two different dipolar relaxation frequencies corresponding to the axial and the cross-sectional directions, which are significantly smaller and larger than the single relaxation frequency of bulk water, respectively. The frequency variation increases as the SWNT diameter decreases. The results suggest that DPS can be used as a fingerprint of water inside SWNTs to monitor the water intrusion into SWNTs.

DOI: 10.1103/PhysRevB.80.045419 PACS number(s): 61.46.Fg, 33.20.Sn, 47.11.Mn, 47.61.−k

I. INTRODUCTION

Single-walled carbon nanotubes (SWNTs) have become a key material in nanotechnology due to their extraordinary properties.[1,2] While variety of applications are extensively explored, carbon nanotubes are expected to play a central role in future nanofluidics applications.[3] As water intrusion into hydrophobic SWNTs has been demonstrated to be possible,[4–6] possibilities of using SWNTs as molecular transporter and filters have been explored with a merit of realizing fast transport even in a nanoscale pore attributing to the exceptionally large slip length at the hydrophobic and atomically smooth interface.[7–10] This motivates studies on the water dynamics in SWNTs, which is expected to be considerably different from that of bulk water.[5,11] Investigations of such hydrodynamics in nanoscale are also important to understand the water transport through aquaporin membrane proteins and ion channels.[12]

Recent developments in the synthesis technique of SWNTs have realized SWNTs film in various morphologies and orientations. Particularly, with molecular transporter and filter applications in mind, aligned carbon nanotube films have strong potential to serve as an ideal nanopore membrane.[8] On the other hand, the local morphologies in the film such as intertube and interbundle spacings and mutiscale defects give rise to uncertainty to the water intrusion into SWNTs. Therefore, it would be extremely useful to be able to monitor the water intrusion into carbon nanotubes. Here, we propose to do so by using the confinement effect on the dielectric permittivity spectra (DPS), particularly the dielectric dipolar relaxation. By indentifying the relaxation frequency shift caused by the confinement, one could probe the presence of water inside carbon nanotube. Furthermore, if the shift can be identified as a function of SWNT diameter, one could even analyze the diameter-dependent water intrusion.

The dynamic and dielectric properties of bulk water have been extensively studied both experimentally and theoretically.[13] A direct modeling of the frequency-dependent dielectric function was suggested by Kim *et al.*,[14,15] which is similar to the integral approach suggested by Wei and Patey.[16] Despite the excellent agreement of the calculated refractive index with the experimental data under certain conditions, due to the complexities of those approaches and difficulties in approximating the integral equation,[15,16] those methods severely lack general feasibility. For example, this method can be barely applied when there are changes in the water temperature and density or when the water is confined in a complex geometry. On the other hand, based on classical mechanics, molecular dynamics (MD) simulations are often used to calculate vibrational spectra and dielectric permittivity of water based on autocorrelation function of velocities and dipole moments,[17–19] owing to their simplicity and feasibility to complex systems.

A few studies on the dynamic properties of water inside and outside SWNTs have been reported,[11,20] which revealed some interesting insights based on the vibration spectra of confined water. In those works, the flexible simple point charged (SPC/F) model was used to describe water molecules and the SWNTs were modeled as rigid tubes by neglecting the dynamics of the carbon atoms. In the current study, we investigate the diameter dependence of vibrational and dielectric permittivity spectra of SPC/E water[21] inside flexible SWNTs modeled by the Brenner potential.[22] Additional simulations with the rigid SWNT assumption are also performed to identify the nontrivial influence of the often-used assumption on the water dynamics. The results demonstrate that the confined dynamics result in strongly anisotropic DPS that are significantly different from those of bulk water. Furthermore, the spectra show strong SWNT-diameter dependence, suggesting that DPS can be used to fingerprint water inside carbon nanotubes.

II. COMPUTATION DETAILS

To investigate the diameter effect on the properties of water inside SWNTs, we performed MD simulations for

TABLE I. Simulated systems.

Tube class	Density (g/cm^3)	Tube diameter (Å)	No. of water
(6,6), flexible	1.0	8.32	11
(6,6), flexible	1.2	8.32	14
(6,6), flexible	1.4	8.32	16
(8,8), flexible	1.0	11.1	44
(8,8), flexible	1.2	11.1	53
(8,8), flexible	1.4	11.1	62
(10,10), flexible	1.0	13.86	98
(10,10), flexible	1.2	13.86	118
(10,10), flexible	1.4	13.86	137
(14,14), flexible	1.0	19.42	270
(14,14), flexible	1.2	19.42	324
(14,14), flexible	1.4	19.42	378
(6,6), rigid	1.4	8.32	16
(8,8), rigid	1.4	11.1	62
(10,10), rigid	1.4	13.86	137
(14,14), rigid	1.4	19.42	378
bulk water	1.0		256

(6,6), (8,8), (10,10), and (14,14) SWNTs, corresponding to diameters of 8.32, 11.1, 13.86, and 19.42 Å. As summarized in Table I, for each SWNT, simulations were performed for three water densities (1, 1.2, and 1.4 g/cm^3). The SWNT length and temperature are 52.81 Å and 300 K, respectively, for all the cases. To examine the effect of SWNT flexibility, simulations with rigid SWNTs with length of 52.81 Å are also carried out for (8, 8), (10, 10), and (14, 14) SWNTs with the water density 1.4 g/cm^3.

The interactions of carbon atoms are modeled by the Brenner potential function.[22] The total potential energy of the system is expressed as

$$E = \sum_i \sum_{j(i<j)} [V_R(r_{ij}) - B_{ij}^* V_A(r_{ij})], \quad (1)$$

where V_R and V_A are the repulsive and attractive potential, respectively, which take a Morse-type form with a certain cutoff function. B_{ij}^* represents the bonding condition of the atoms. The set of parameters which reproduces the force constant better is used.[22] The parameter set also reproduces SWNT phonon dispersion relations with sufficient accuracy.[23] A water molecule is modeled by SPC/E,[21] which is a rigid water model known for accurately reproducing potential energy and dielectric constant.[17,18] SPC/E potential is expressed as the superposition of Lennard-Jones potential of oxygen-oxygen interaction and the electrostatic potential by charges on oxygen and hydrogen as follows:

$$\phi_{12} = 4\varepsilon_{oo}\left[\left(\frac{\sigma_{oo}}{R_{12}}\right)^{12} - \left(\frac{\sigma_{oo}}{R_{12}}\right)^{6}\right] + \sum_i \sum_j \frac{q_i q_j e^2}{4\pi\varepsilon_0 r_{ij}}, \quad (2)$$

where R_{12} denotes the distance between oxygen atoms and $\sigma_{oo}=3.166$ Å and $\varepsilon_{oo}=0.650$ kJ/mol are the Lennard-Jones parameters. The coulombic interaction is the sum of nine pairs of point charges, where r_{ij} denotes the distance between intermolecular point charges. The model system has been previously used to simulate the phase change in water inside an SWNT and the anomalous diameter dependence of the freezing temperature to the ice nanotube[4,24] was successfully reproduced.[25]

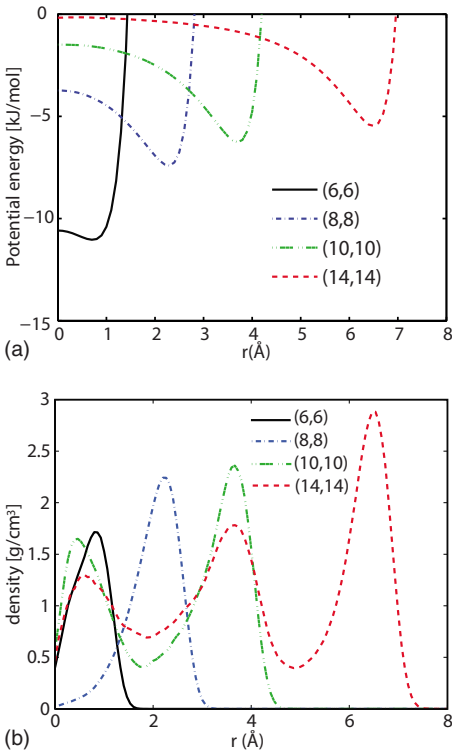

FIG. 1. (Color online) Potential energy and density profiles. (a) Water-SWNT potential energy as a function of the distance from the SWNT axis. (b) Water density as a function of distance from the SWNT axis.

Periodic boundary conditions are applied in the simulations with the long-range electrostatic interactions of water molecules treated by the Ewald method.[26,27] The Verlet integration method is employed with a time step 0.5 fs to solve the momentum equations. The system was equilibrated for the first 50 ps by applying the velocity-scaling method and then data were sampled for 600 ps under microcanonical ensembles.

In the MD simulations, the interaction between oxygen and carbon atoms is modeled by a Lennard-Jones potential. The parameters for the Lennard-Jones potential are $\sigma_{oc}=3.19$ Å and $\varepsilon_{oc}=0.3126$ kJ/mol. The density of water inside an SWNT was determined based on the effective internal volume, whose radius is defined as the distance from the SWNT axis to the position where the water-SWNT potential is zero.[11] As seen in the water-SWNT potential profile in Fig. 1(a), the thickness of the positive potential layer at the hydrophobic surface is approximately 2.72 Å and is independent of the SWNT diameter.

III. RESULTS AND DISCUSSIONS

A. Water structures

First, we examine the structure of water molecules inside SWNTs, which plays important roles in understanding the

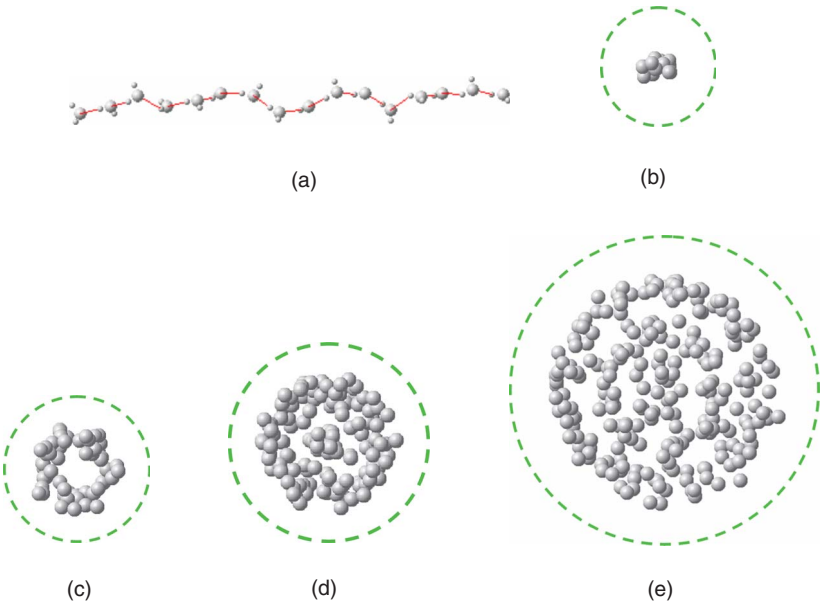

FIG. 2. (Color online) Water inside SWNTs with different diameters. Water inside a (6,6) SWNT; (a) side view and (b) cross-sectional view. Water inside (c) a (8,8) SWNT, (d) a (10,10) SWNT, and (e) a (14,14) SWNT. For (b)–(e), only the oxygen atoms are shown for clarity. The dotted lines denote the averaged SWNT profiles.

water dynamics. The time-averaged oxygen density distributions as functions of the distance from the SWNT axis are shown in Fig. 1(b) for various SWNT diameters. The profiles are similar to those of SPC/F water inside rigid SWNTs,[28] though the peak positions are slightly upshifted in the current system due to the flexibility of the SWNTs. The corresponding instantaneous structures of water molecules are also shown in Fig. 2. In a (6,6) SWNT, water molecules form a chain [Figs. 2(a) and 2(b)] with their mass centers located away from the SWNT axis. In a (8, 8) SWNT, water molecules appear as a single cylindrical layer [Fig. 2(c)] and in a (10, 10) SWNT, there is an additional water chain within a cylindrical layer [Fig. 2(d)]. Finally, inside a (14, 14) SWNT, two confocal cylindrical layers and a chain in the center are formed [Fig. 2(d)].

The simulations for different water densities (1, 1.2, and 1.4 g/cm^3) show that at least density of 1.4 g/cm^3 is needed to fill all the SWNTs with water, except for (6, 6) SWNT, which was partially filled for all the parameters tested in the current study (Table I).

B. Vibrational spectra

The velocity power spectrum of atoms is an essential tool to elucidate the molecular dynamics from the simulated trajectories, though the profiles cannot be directly compared with experimental measurements. A spectrum can be calculated from the normalized velocity autocorrelation function of atoms,[19]

$$S(\omega) = \int_0^\infty dt C_N(t) \cos\ \omega t, \tag{3}$$

$$C(t) = \frac{\langle \vec{v}(t) \cdot \vec{v}(t) \rangle}{\langle \vec{v}(0\ \ \cdot \vec{v}(0) \rangle}, \tag{4}$$

where $\vec{v}(t)$ is the collective velocity of atoms and $C(t)$ is the normalized velocity autocorrelation functions of the target atoms. All SWNTs are arranged parallel to Z direction and therefore the cross section is in the XY plane. The power spectra in the XY plane and along the Z direction are defined, respectively, as

$$S_{xy}(\omega) = \int_0^\infty dt C_{N,xy}(t) \cos\ \omega t,$$

$$C_{N,xy}(t) = \frac{v_x(t)v_x(0) + v_y(t)v_y(0)}{v_x(0)v_x(0) + v_y(0)v_y(0)} \tag{5}$$

$$S_z(\omega) = \int_0^\infty dt C_{N,z}(t) \cos\ \omega t, \quad C_{N,z}(t) = \frac{v_z(t)v_z(0)}{v_z(0)v_z(0)}. \tag{6}$$

The spectra calculated from the velocities of oxygen and hydrogen atoms are denoted with subscripts O and H, respectively. The current analyses indicate that the differences in water density have minor effects on $S_H(\omega)$ and $S_O(\omega)$, and hence only results of water with density of 1.4 g/cm^3 are presented here.

In Fig. 3(a), the oxygen vibrational spectra $S_O(\omega)$ are plotted for various SWNT diameters, clearly exhibiting the confinement effects. The result qualitatively agrees well with the spectra reported by Marti and Gordillo[11] despite the difference in water model, density of water, and flexibility of SWNTs. The two main bands appearing as a distinct peak around 50 cm^{-1} (B band) and a shoulder in 200–300 cm^{-1} (S band) originate from the bending and stretching of hydrogen bonds, respectively.[29] The confinement effect can be clearly observed in the spectra, particularly for the case of (6, 6) SWNT, where the confinement increases and decreases the intensity of B band and S band, respectively. More insights into the confinement effect can be gained by decomposing the spectra into axial and cross-sectional directions as shown Fig. 3(b) taking the case of (6, 6) SWNT. The figure demonstrates a large anisotropy in the power spectra, where the intensity enhancement of B band takes place mainly in

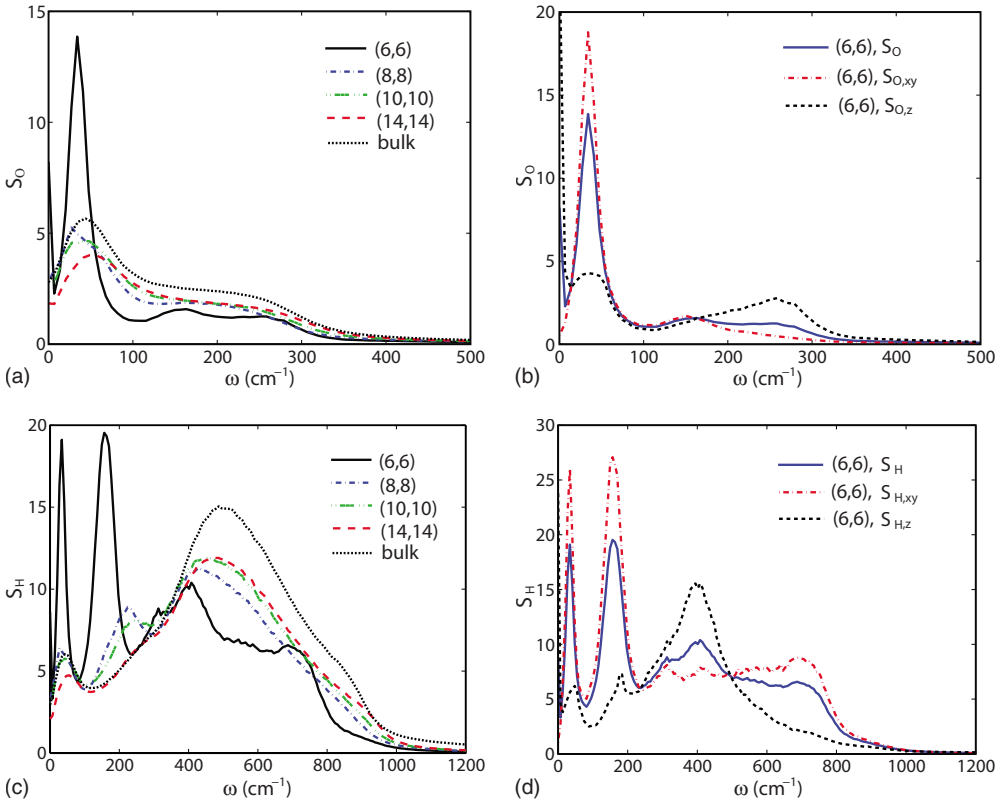

FIG. 3. (Color online) Power spectra of hydrogen and oxygen atoms for various SWNT diameters. (a) $S_O(\omega)$ for various SWNT diameters. (b) $S_O(\omega)$ for (6,6) SWNT. (c) $S_H(\omega)$ for various SWNT diameters. (d) $S_H(\omega)$ for (6,6) SWNT.

XY plane while *S*-band intensity is higher in the *Z* direction. It is understandable that the stretching of hydrogen bonds mainly takes place along the *Z* direction as the water molecules are forced to align along the SWNT. Such alignment also restricts the bending of hydrogen network in the cross-sectional plane and the destabilized hydrogen bonding makes the longitudinal motion of water more volatile resulting in higher spectral intensity in *B* band.

Hydrogen power spectra illustrate the confinement effect on librations of water molecules. As shown in Fig. 3(c) S_H of water inside SWNT departs from that of bulk water with decreasing the SWNT diameter. It also shows that all the peaks exhibit redshift implying the softer dynamics with enhancing the confinement. Most noticeable feature of the spectra is that the confined water exhibits a band around 200 cm^{-1} which is absent in the bulk water spectrum. This band is related to the frustrated translation of water[30] and has been associated with motion of dangling nonbonded hydrogen in case of water on graphite surface by Marti and Gordillo.[31] This agrees with the current results, where the intensity of the band around 200 cm^{-1} is much stronger in $S_{H,xy}(\omega)$ than in $S_{H,z}$ as shown in Fig. 3(d) for the (6, 6) SWNT case.

The libration band (350–800 cm^{-1}) of water inside SWNT has less intensity than that of bulk water due to variations in the frustrated rotational motion. For bulk water, the libration band consists of two different modes corresponding to different vibrational modes of the hydrogen-bonded structures.[32] While the water inside an SWNT also exhibits multimode nature of libration, as seen in Fig. 3(d) for the (6, 6) SWNT case, $S_{H,z}$ has a strong distinct peak at around 400 cm^{-1} and $S_{H,xy}(\omega)$ has a broader band with a shoulder around 700 cm^{-1}. The libration of water inside SWNT is highly anisotropic since the degree of frustration depends on the direction of rotation. This also indicates that the different libration modes manifests in different directions implying that the libration modes (eigenvectors) are oriented along and normal to the SWNT. This is consistent with the observation of aligned water structure inside the SWNT shown in Fig. 2(a).

C. Dielectric properties

The static dielectric permittivity of isotropic bulk water can be calculated by the following expression[18,19,27]

$$\varepsilon_0 = 1 + \frac{4\pi}{3Vk_BT}\phi^c(0), \tag{7}$$

where V, k_B, and T are the effective internal volume, Boltzmann constant, and temperature. ϕ^c is the collective time-correlation function of dipole moments and expressed as

$$\phi^c(t) = \langle \vec{M}(t) \cdot \vec{M}(0) \rangle, \tag{8}$$

where $\vec{M}(t) = \Sigma_{i=1}^{N} \vec{\mu}_i(t) = (M_x, M_y, M_z)^T$ and $\vec{\mu}_i$ is the dipole moment of the ith molecule.

Due to the confinement inside SWNTs, it is expected that water exhibits anisotropic dielectric properties. Therefore, we define an effective static constant for anisotropic cases as

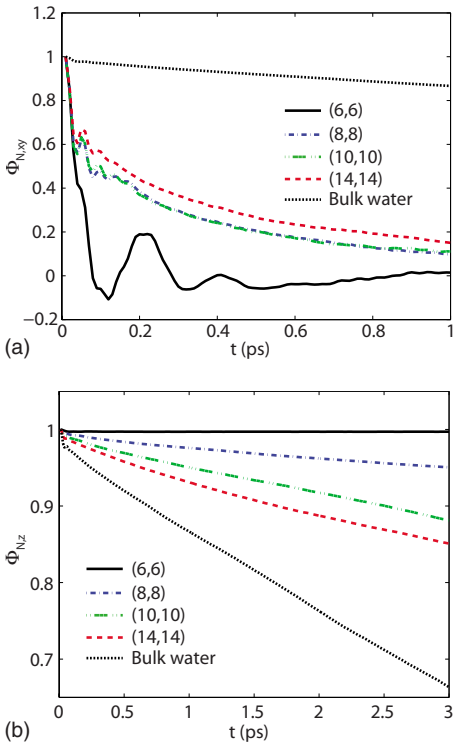

FIG. 4. (Color online) Collective DACF; (a) $\phi_{N,xy}(t)$ and (b) $\phi_{N,z}(t)$.

$$\varepsilon_0 = \frac{2\varepsilon_{0,xy} + \varepsilon_{0,z}}{3}, \quad \varepsilon_{0,xy} = 1 + \frac{2\pi}{Vk_BT}\phi^c_{xy}(0),$$

$$\varepsilon_{0,z} = 1 + \frac{4\pi}{Vk_BT}\phi^c_z(0).$$

Here, $\varepsilon_{0,xy}$ is the cross-sectional permittivity and $\varepsilon_{0,z}$ is the axial permittivity calculated from $\phi^c_{xy}(0)=\langle M_x(0)^2+M_y(0)^2\rangle$ and $\phi^c_z(0)=\langle M_z(0)^2\rangle$. For isotropic bulk water, $\varepsilon_0=\varepsilon_{0,xy}=\varepsilon_{0,z}$.

The calculation of the DPS is based on the static permittivity ε_0 and the normalized collective dipole moment autocorrelation function (DACFs), which takes the forms

$$\phi^C_{N,xy}(t) = \frac{\langle \vec{M}_{xy}(t)\cdot\vec{M}_{xy}(0)\rangle}{\langle \vec{M}_{xy}(0)\cdot\vec{M}_{xy}(0)\rangle}, \quad \phi^C_{N,z}(t) = \frac{\langle M_z(t)\cdot M_z(0)\rangle}{\langle M_z(0)\cdot M_z(0)\rangle},$$

where $\vec{M}_{xy}=(M_x,M_y)^T$.

Figure 4 shows the collective DACFs for water inside flexible SWNTs with density 1.4 g/cm^3 together with that of bulk water. In Fig. 4(a), it is observed that the relaxation of $\phi^C_{N,xy}(t)$ is fastest for water inside a (6,6) SWNT and slowest for water inside a (14,14) SWNT. In case of (8,8) and (10,10) SWNTs, $\phi^C_{N,xy}(t)$ shows similar relaxation characteristics. For all the SWNTs tested, the DACF in the XY plane relaxes significantly faster than that of bulk water.

In Fig. 4(b), the collective DACFs of water inside SWNTs along the Z direction, $\phi^C_{N,z}(t)$, are plotted together with the isotropic values of bulk water. We see that the relaxation of water inside SWNTs is always slower than that of bulk water. For a (6,6) SWNT, along the Z direction, the relaxation of water is so slow that a converged value could not be obtained within the current simulation time. We attribute this dramatically slow relaxation to the large amount of hydrogen-bond losses due to the contact of water and hydrophobic SWNT. It was observed that more than 50% of hydrogen atoms of the water chain inside (6,6) SWNTs are nonbonded, which makes the atoms extremely unstable. As the diameter of SWNTs increases, the relaxation becomes faster.

TABLE II. Static dielectric permittivities and relaxation times.

SWNT class	$\varepsilon_{0,xy}$	$\varepsilon_{0,z}$	ε_0	τ_{xy} (ps)	τ_z (ps)
(8,8) flexible	6.28	256.03	89.53	0.48	39.34
(10,10) flexible	6.12	202.59	71.60	0.43	19.60
(14,14) flexible	5.81	171.93	61.18	0.59	18.34
(8,8) rigid	6.32	531.00	181.21	0.40	29.12
(10,10) rigid	6.07	205.25	72.46	0.43	12.73
(14,14) rigid	5.92	142.12	51.32	0.64	15.43

The static dielectric permittivity and the relaxation time of water inside SWNTs with chiralities (8,8), (10,10), and (14,14) are summarized in Table II. Here we pay particular attention to the density 1.4 g/cm^3 cases, where all the SWNTs with the three chiralities were filled with water. Although, in principle, we could also calculate the static permittivity of water inside a (6,6) SWNT, the value hardly converges along the axial direction due to its extremely long relaxation time. For all the above three chiralities, the static dielectric permittivity in the cross-plane $\varepsilon_{0,xy}$ and the corresponding relaxation time τ_{xy} (about 0.5 ps) are severely suppressed (to about 6) compared with those of bulk water. No obvious dependence on the SWNT diameter and flexibility are observed in the XY plane.

On the other hand, in the axial direction, confined water possesses higher static permittivity. The effect of SWNT diameter on $\epsilon_{0,z}$ is clearer as plotted in Fig. 5, where $\epsilon_{0,z}$ decreases as the SWNT diameter increases. This reflects that the dipoles of water confined in SWNTs with small diameters are more strongly forced to align parallel to the axial direction than in SWNTs with large diameters. Figure 5 also

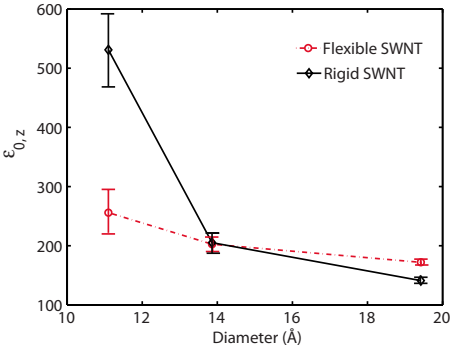

FIG. 5. (Color online) SWNT-diameter effects on the static dielectric permittivity and influence of the SWNT flexibility.

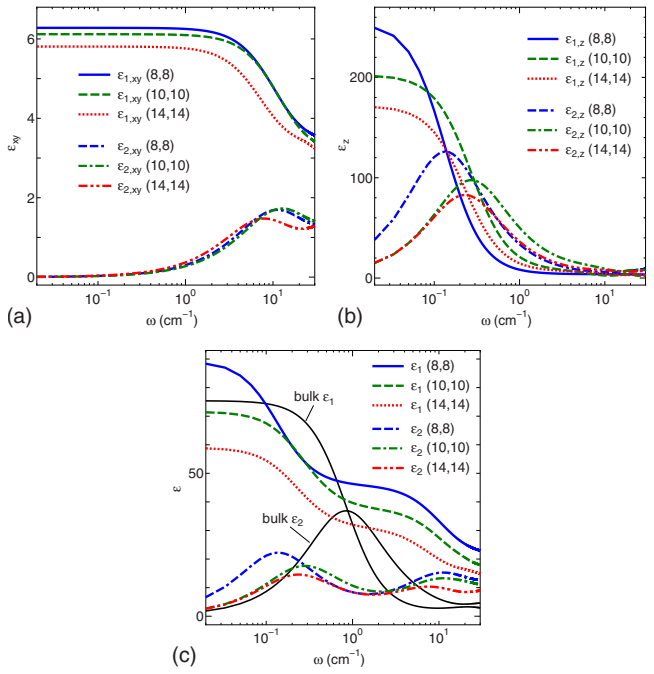

FIG. 6. (Color online) DPS of water inside flexible SWNTs. (a) DPS in the *XY* plane. (b) DPS along the *Z* direction. (c) Effective DPS.

shows that the diameter effect can be severely exaggerated by the rigid nanotube assumption for diameter as small as that of a (8,8) SWNT. The difference between rigid and flexible SWNT cases decreases as the diameter increases. The presence of lattice vibrations, particularly those associated with low frequency and small wave-number phonons, is expected to affect the effective local volume and therefore to influence the confinement effect. This is consistent with the observation from Fig. 5, where the confinement effect in the flexible SWNT is weaker than in the rigid one.

The complex-frequency-dependent dielectric permittivity spectrum (DPS) is expressed as $\varepsilon(\omega)=\varepsilon_1(\omega)-i\varepsilon_2(\omega)$, where ε_1 is the real part and ε_2 is the imaginary part. These functions in the *XY* plane and along the *Z* direction are related to the Fourier transform of $\phi^c_{N,xy}(t)$ and $\phi^c_{N,z}(t)$ by

$$\varepsilon_{1,xy}(\omega) = \varepsilon_{0,xy} - (\varepsilon_{0,xy} - 1)\omega \int_0^\infty \phi^c_{N,xy}(t)\sin\ \omega t dt, \quad (9)$$

$$\varepsilon_{2,xy}(\omega) = (\varepsilon_{0,xy} - 1)\omega \int_0^\infty \phi^c_{N,xy}(t)\cos\ \omega t dt, \quad (10)$$

$$\varepsilon_{1,z}(\omega) = \varepsilon_{0,z} - (\varepsilon_{0,z} - 1)\omega \int_0^\infty \phi^c_{N,z}(t)\sin\ \omega t dt, \quad (11)$$

$$\varepsilon_{2,z}(\omega) = (\varepsilon_{0,z} - 1)\omega \int_0^\infty \phi^c_{N,z}(t)\cos\ \omega t dt. \quad (12)$$

Figure 6 shows the DPS of water inside flexible SWNTs with different diameters. To calculate the Fourier transform of $\phi_N(t)$, fitting was performed on the DACF computed for 600 ps, following the method described by English and Macelroy.[18] The raw data from $t=0$ to $t=0.5$ ps were approved for the short-time behavior and the data from $t=0.5$ ps to $t=600$ ps were fitted to $A\exp(-t\tau_D)$ to characterize the long-time behavior, where τ_D is the Debye relaxation time. The Fourier transform is performed for this partially fitted DACF instead of the raw data to calculate the dynamic dielectric constant. As shown in Fig. 6(a), in the *XY* plane, the maximum magnitude of dielectric permittivity is less than seven and the relaxation frequencies are around 10 cm^{-1}. The DPS of water inside SWNTs along the *Z* direction [Fig. 6(b)] shows that when the diameter increases, the relaxation frequencies increase, and the magnitudes of permittivity decrease.

From Fig. 6, we observe that the static permittivity decreases with increasing SWNT diameter. Figure 6(c) shows that ϵ_0 of water inside (8,8) SWNT is larger than bulk water while inside (10,10) and (14,14) SWNTs it is smaller than bulk water. This can be explained by percent of the nonbonded hydrogen atoms in the systems, which is about 28%, 32%, 21%, and 15% for bulk water, inside (8,8), (12,12), and (14,14) SWNTs, respectively, in our calculation. Here, we adopted the geometrical criteria[33] to describe a hydrogen bond, i.e., the distance between a hydrogen atom and an oxygen atom is less than 2.4 Å, and the distance between the two oxygen atoms is less than 3.6 Å. Note that hydrogen bonds in liquid water prevent the reorientation of a molecular dipole and ϵ_0 is defined in terms of the fluctuation of the sum of dipoles in the system.

Having an isotropic measurement of dielectric function in mind, the real and imaginary parts of effective DPS are calculated as

$$\varepsilon_1(\omega) = \varepsilon_0 - (\varepsilon_0 - 1)\omega \int_0^\infty \phi^c_N(t)\sin\ \omega t dt, \quad (13)$$

$$\varepsilon_2(\omega) = (\varepsilon_0 - 1)\omega \int_0^\infty \phi^c_N(t)\cos\ \omega t dt, \quad (14)$$

which are plotted in Fig. 6(c). The permittivity of bulk water is also plotted for comparison. The ε_0 of bulk water is about 74, which is in good accord with the experimental data 80,[13] and the relaxation time τ_D is about 7 ps, which is close to the simulation result by English and Macelroy.[18] As for the water confined in SWNTs, the spectra exhibit two relaxation frequencies corresponding to the axial and cross-sectional directions. The relaxation frequency is related to the Debye relaxation time by $f \sim 1/\tau_D$. Two different frequencies appear because a water molecule electrostatically interacts with much more other water molecules in the *Z* direction than in the *XY* plane due to the quasi-one-dimensional structure. Therefore, with the increase in the diameter of the SWNTs, the interval between two frequencies decreases because the number of coulombic interactions among water molecules in the *XY* plane increases.

IV. CONCLUSION

We have performed MD simulations of water inside SWNTs to investigate the anisotropic dynamic and dielectric

properties of water under nanoscale confinement. The model system takes the dynamics of the SWNT into account, which was found to be important in case of small diameter SWNTs. The directional vibrational spectra of oxygen and hydrogen atoms provide rich insight into the anisotropic dynamics of hydrogen-bonded water with directional frustration and destabilization imposed by the confinement. Strong anisotropy was also observed in the static permittivity, where the value along the axial direction is much larger than that in the cross-section plane due to the orientational alignment of the water dipoles. The overall DPS identified two relaxation frequencies related to the two components of axial and cross-sectional directions due to the quasi-one-dimensional water structure, where a water molecule electrostatically interacts with much less water molecules in the cross-sectional plane than along the axial direction. This results in the diameter-dependent relaxation frequencies, and thus, suggests that DPS can be used as a fingerprint of water inside SWNTs to monitor the water intrusion into SWNTs.

ACKNOWLEDGMENTS

This work is supported in part by the Swedish Research Council (VR) and the Japan Society for the Promotion of Science (JSPS), Grants-in-Aid for Scientific Research 19051016 and 19860022. The Swedish National Infrastructure for Computing (SNIC) is also acknowledged for computer resources.

*yuan.lin@sintef.no
†shiomi@photon.t.u-tokyo.ac.jp

[1] R. Saito, G. Dresselhaus, and M. S. Dresselhaus, *Physical Properties of Carbon Nanotube* (Imperial College, London, 1998).
[2] A. Jorio, G. Dresselhaus, and M. S. Dresselhaus, *Carbon Nanotubes: Advanced Topics in the Synthesis, Structure, Properties and Applications* (Springer-Verlag, Berlin, 2008).
[3] A. Noy, H. G. Park, F. Fornasiero, J. K. Holt, C. P. Grigoropoulos, and O. Bakajin, Nanotoday **2**, 22 (2007).
[4] Y. Maniwa, H. Kataura, M. Abe, A. Udaka, S. Suzuki, Y. Achiba, H. Kira, K. Matsuda, H. Kadowaki, and Y. Okabe, Chem. Phys. Lett. **401**, 534 (2005).
[5] A. I. Kolesnikov, J.-M. Zanotti, C.-K. Loong, P. Thiyagarajan, A. P. Moravsky, R. O. Loutfy, and C. J. Burnham, Phys. Rev. Lett. **93**, 035503 (2004).
[6] N. Naguib, H. Ye, Y. Gogotsi, A. G. Yazicioglu, C. M. Megaridis, and M. Yoshimura, Nano Lett. **4**, 2237 (2004).
[7] M. Majumder, N. Chopra, R. Andrews, and B. J. Hinds, Nature (London) **438**, 44 (2005).
[8] J. K. Holt, H. G. Park, Y. Wang, M. Stadermann, A. B. Artyukhin, C. P. Grigoropoulos, A. Noy, and O. Bakajin, Science **312**, 1034 (2006).
[9] J. A. Thomas and A. J. H. McGaughey, Nano Lett. **8**, 2788 (2008).
[10] J. Shiomi and S. Maruyama, Nanotechnology **20**, 055708 (2009).
[11] J. Marti and M. C. Gordillo, J. Chem. Phys. **114**, 10486 (2001).
[12] M. S. P. Sansom and P. C. Biggin, Nature (London) **414**, 156 (2001).
[13] J. N. Murrell and A. D. Jenkins, *Properties of Liquids and Solutions*, (Chichester, England, 1994).
[14] S. H. Kim, G. Vignale, and B. DeFacio, Phys. Rev. A **46**, 7548 (1992).
[15] S. H. Kim, G. Vignale, and B. DeFacio, Phys. Rev. E **50**, 4618 (1994).
[16] D. Wei and G. N. Patey, J. Chem. Phys. **91**, 7113 (1989).
[17] J. Anderson, J. J. Ullo, and S. Yip, J. Chem. Phys. **87**, 1726 (1987).
[18] N. J. English and J. M. Macelroy, Mol. Phys. **100**, 3753 (2002).
[19] J. Marti, E. Guardia, and J. A. Padro, J. Chem. Phys. **101**, 10883 (1994).
[20] M. C. Gordillo and J. Marti, Phys. Rev. B **67**, 205425 (2003).
[21] H. J. C. Berendsen, J. R. Grigera, and T. P. J. Straatsma, J. Phys. Chem. **91**, 6269 (1987).
[22] D. W. Brenner, Phys. Rev. B **42**, 9458 (1990).
[23] J. Shiomi and S. Maruyama, Phys. Rev. B **73**, 205420 (2006).
[24] K. Koga, G. T. Gao, H. Tanaka, and X. C. Zeng, Nature (London) **412**, 802 (2001).
[25] J. Shiomi, T. Kimura, and S. Maruyama, J. Phys. Chem. C **111**, 12188 (2007).
[26] D. M. Heyes, CCP5 NewsLetters **8** (1983).
[27] M. P. Allen and D. J. Tildeslley, *Computer Simulation of Liquids* (Oxford Science Publication, New York, 1987).
[28] J. Marti and M. C. Gordillo, Phys. Rev. E **64**, 021504 (2001).
[29] G. E. Walrafen, in *Water: A Comprehensive Treatise*, edited by F. Franks (Plenum, New York, 1972).
[30] P. A. Thiel and T. E. Madey, Surf. Sci. Rep. **7**, 211 (1987).
[31] M. C. Gordillo and J. Marti, J. Chem. Phys. **117**, 3425 (2002).
[32] G. E. Walrafen, J. Chem. Phys. **40**, 3249 (1964).
[33] J. Marti, J. Chem. Phys. **110**, 6876 (1999).